

Journal of Mechanics of Materials and Structures

**A COUPLED HONEYCOMB COMPOSITE SANDWICH BRIDGE-VEHICLE
INTERACTION MODEL**

Mijia Yang and A. T. Papagiannakis

Volume 5, No. 4

April 2010

A COUPLED HONEYCOMB COMPOSITE SANDWICH BRIDGE-VEHICLE INTERACTION MODEL

MIJIA YANG AND A. T. PAPAGIANNAKIS

This paper presents a coupled, dynamic vehicle and honeycomb composite sandwich bridge deck interaction model. The composite sandwich deck consists of E-glass fibers and polyester resin. Its core consists of corrugated cells in a sinusoidal configuration along the travel direction. First, analytical predictions of the effective flexural and transverse shear stiffness properties of the sandwich deck were obtained in the longitudinal and transverse directions. These were based on the modeling of equivalent properties for the face laminates and core elements. Using the first order shear sandwich theory, the dynamic response of the sandwich deck was analyzed under moving dynamic loads. A dynamic vehicle simulation model was used for the latter, assuming that the deck response is the only source of excitation (i.e., its roughness was assumed to be negligible). Subsequently, the dynamic load factors of the sandwich bridge deck were calculated for different traveling velocities. The results suggest that the dynamic load factors vary with the traveling speed and increase significantly with decreasing deck stiffness. Considering multiple degrees of freedom for the vehicle further amplifies the dynamic loading factor and increases the vibration generated by vehicles.

Introduction

Sandwich elements are commonly used in aerospace and automobile structures since they offer great energy absorption and higher moment of inertia without imposing a significant weight penalty. Recently, growing civil engineering infrastructure rehabilitation needs suggest that innovative deck materials such as fiber-reinforced polymer (FRP) composite sandwich structures may be suitable for bridge decks [Plunkett 1997; Davalos et al. 2001]. These structures typically consist of a corrugated or closed-cell core encased between two face sheets. Such systems are lightweight while providing high strength. Keller [2001] also conducted a series of laboratory and field experiments of FRP bridges and verified that the sandwich elements, if well designed, can be implemented as bridge decks.

However, the performance of sandwich decks for different core configurations and loading cases is not fully understood. Davalos et al. [2001] conducted a performance evaluation of the FRP sandwich panels with a sinusoidal honeycomb core. Xu et al. [2001] proposed an analytical method to estimate the core transverse shear stiffness. Librescu and Hause [2000] reported their research in the modeling of the advanced sandwich structures, especially the study of stability behavior of sandwich panels. Analysis of modern sandwich panels was done in [Frostig 2003; Frostig and Thomsen 2004] using both classical and high-order models. This work studied in-plane and out-of-plane displacement patterns and stress distributions in the sandwich panels under various boundaries and loading conditions.

Keywords: Vehicle-bridge interaction, dynamic loading factor, sandwich structures, stiffness.

There is considerably less literature on the dynamic response of sandwich structures, especially under forced vibrations. Most recently, dynamic response models of higher-order sandwich panels with flexible core were developed in [Yang and Qiao 2005a]. These were used to study free vibration, impact behavior, and stress wave propagation in a sandwich beam. However, in order to safely design and implement sandwich panels as bridge decks, the dynamic response and its dynamic load factor of a sandwich deck under moving forces need to be studied.

This paper describes a comprehensive approach to predicting the dynamic response of thick sandwich bridge deck. In addition, it compares their dynamic loading factors to those of conventional concrete decks. First, the analytical stiffness properties of the face sheets and the core of the sandwich structures are estimated using the micro/macromechanics method [Davalos et al. 1996]. The stiffness properties of whole sandwich panel are then evaluated by modeling the sandwich panel as a three-layer laminated structure, and the estimated stiffness properties are subsequently used for predicting the dynamic responses of FRP sandwich bridge decks. A semi-analytical relationship between the mechanical properties and the dynamic response of the sandwich deck is finally developed. Based on this relationship, the dynamic loading factor impacted by traveling vehicles is evaluated and used in analyzing composite sandwich bridge decks.

1. Effective flexural and shear stiffness of sandwich decks

The first step in designing a composite sandwich deck is the estimation of the equivalent stiffness properties of the face sheets, the core elements, and the sandwich deck. The configuration of the face laminate, sinusoidal core, and sandwich panels are summarized in Figure 1.

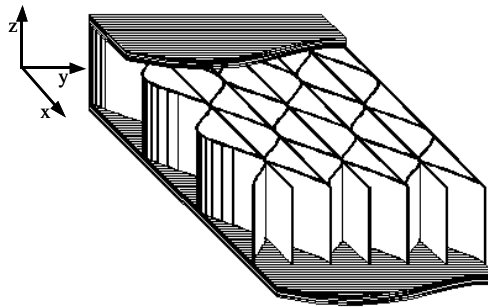


Figure 1. Configuration of sandwich panel.

1.1. Modeling of face laminates. The engineering properties of laminated panels can be predicted by a combined micro/macromechanics approach [Davalos et al. 1996]. The prediction of the ply properties using the micromechanics approach is well defined [Chamis 1984]. The stiffness properties of each layer can be computed from existing micromechanics models, such as rule of mixtures (ROM) [Jones 1999], periodic microstructure (PM) [Luciano and Barbero 1994] and composite cylinders (CC) [Hashin and Rosen 1964], wherein each layer is modeled as a homogeneous, linearly elastic, and generally orthotropic material. As in [Davalos et al. 2001], a typical face laminate may include the following four types of fiber layers:

Ply name	Orientation	E_1 (GPa)	E_2 (GPa)	G_{12} (GPa)	G_{23} (GPa)	ν_{12}	ν_{23}
bond layer	random	9.72	9.72	3.50	2.12	0.394	0.401
CM3205	0° or 90°	27.72	8.00	3.08	2.88	0.295	0.390
	random	11.79	11.79	4.21	2.36	0.402	0.400
UM1810	0°	30.06	8.55	3.30	3.08	0.293	0.386
	random	15.93	15.93	5.65	2.96	0.409	0.388
core mat	random	11.79	11.79	4.21	2.97	0.402	0.388

Table 1. Ply stiffness properties obtained from micromechanics model.

- (1) Chopped strand mat (ChopSM), which is made of short fibers randomly oriented, resulting in nearly isotropic in-plane properties.
- (2) Continuous strand mat (ContSM) which consists of continuous randomly oriented fibers; this product is commonly used as backing material for non-woven fabrics and can be modeled as an isotropic layer.
- (3) Bidirectional stitched fabrics (SF) with balanced off-angle unidirectional fibers (e.g., 0°/90° or ±45°).
- (4) Unidirectional layer of fiber bundles or rovings.

The stiffness of each ply can be predicted from micromechanics models. In this study, a micromechanics model for composites with periodic microstructure [Luciano and Barbero 1994] is used to obtain the elastic constants for each individual layer (Table 1).

After the elastic properties of each ply are obtained from micromechanics, the equivalent stiffness properties of the face laminate are computed from classical lamination theory [Jones 1999]. A set of equivalent laminate stiffness properties can be defined for approximately balanced symmetric face laminates [Davalos et al. 1996] and are given in Table 2. These elastic constants (e.g., E_x^f , E_y^f , G_{xy}^f , and ν_{xy}^f) represent the stiffness of an equivalent orthotropic plate that behaves like the actual laminate under out-of-plane and in-plane loads.

1.2. Modeling of honeycomb core. Unlike traditional honeycomb sandwich structures, the shape of the corrugated cell wall in the sandwich is defined by a sinusoidal function (Figure 1).

An example of a honeycomb core manufactured by Kansas Structural Composites, Inc. (KSCI, Russell, Kansas) is shown in Figure 2, and the dimensions of the sinusoidal core are $h = 25.4$ mm (1.0 in) and $b = 50.8$ mm (2.0 in). In the coordinate system shown in Figure 2, the wave function of a corrugated

E_x^f	E_y^f	ν_{xy}^f	G_{xy}^f	G_{xz}^f	G_{yz}^f
19.62 GPa	12.76 GPa	0.302	3.76 GPa	3.75 GPa	3.68 GPa
2.85×10^6 psi	1.85×10^6 psi		0.55×10^6 psi	0.54×10^6 psi	0.53×10^6 psi

Table 2. Material properties of face laminates.

$$N = \frac{Fb + Ph\pi \sin(\pi x/b)}{b\sqrt{1 + (h\pi/b)^2 \sin^2(\pi x/b)}}, \tag{3}$$

$$V = \frac{Fh\pi \sin(\pi x/b) - Pb}{b\sqrt{1 + (h\pi/b)^2 \sin^2(\pi x/b)}}. \tag{4}$$

The elastic strain energy of the curved wall in **Figure 3** is expressed as

$$U = \int_0^S \left(\frac{\alpha_M M^2}{2} + \frac{\alpha_N N^2}{2} + \frac{\alpha_V V^2}{2} \right) ds, \tag{5}$$

where

$$\alpha_M = \frac{12}{E_1 t_2^3}, \quad \alpha_N = \frac{1}{E_1 t_2}, \quad \alpha_V = \frac{1}{\kappa G_{13} t_2}. \tag{6}$$

Castigliano’s theorem gives

$$\frac{\partial U}{\partial M_0} = 0, \quad \frac{\partial U}{\partial P} = \Delta_y, \quad \frac{\partial U}{\partial F} = \Delta_x. \tag{7}$$

It is noted that

$$\Delta_x = -\frac{2Fb}{E_1 t_1}. \tag{8}$$

Combining (7) and (8) gives the expression of Δ_y in term of P . Therefore, the core effective transverse Young’s modulus (E_y^e) is obtained as

$$E_y^e = \frac{\sigma_y}{\varepsilon_y} = \frac{P/b}{\Delta_y/2h} = \frac{2Ph}{b\Delta_y}. \tag{9}$$

Similarly, a macroscopic stress σ_x is applied to the unit cell to compute the core effective longitudinal Young’s modulus in the x direction (**Figure 4**). Again, due to the symmetry of the unit cell, only a quarter of it is modeled (**Figure 4**, left). Its internal forces and moment can be obtained with the aid of **Figure 4**, right.

The strain energy of the quarter representative volumetric element (RVE) is given as

$$U = \int_0^S \left(\frac{\alpha_M M^2}{2} + \frac{\alpha_N N^2}{2} + \frac{\alpha_V V^2}{2} \right) ds + \frac{F_1^2 b}{E_1 t_1} + \frac{F_3^2 b}{E_1 t_1}, \tag{10}$$

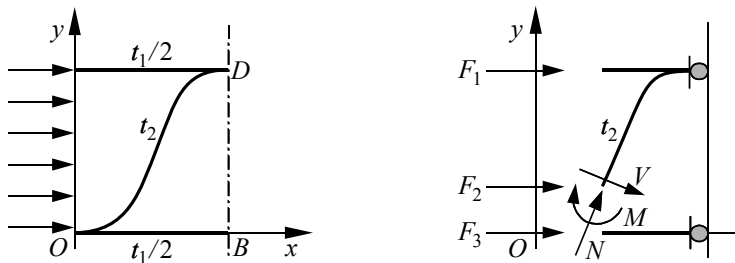


Figure 4. Modeling of the core effective longitudinal Young’s modulus, E_x^e : loading configuration (left) and internal force analysis (right).

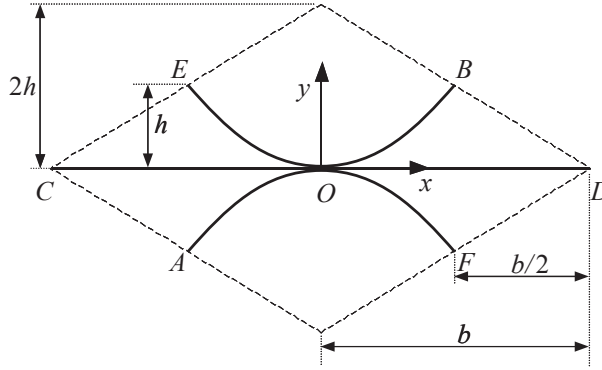


Figure 5. Unit cell of sinusoidal core for out-of-plane shear moduli.

where M is the internal moment and N , and V are the internal forces of the half curve waved wall and are calculated by using (2)–(4) with $P = 0$.

Again, invoking Castigliano’s theorem results in

$$\frac{\partial U}{\partial M_0} = 0, \quad \frac{\partial U}{\partial F_1} = \Delta_x, \quad \frac{\partial U}{\partial F_2} = \Delta_x, \quad \frac{\partial U}{\partial F_3} = \Delta_x, \quad (11)$$

where F_1 , F_2 , and F_3 correspond to the forces on the top flat, curved, and bottom flat walls, respectively (see Figure 4, right), and can be expressed in term of Δ_x . Hence, the core effective longitudinal Young’s modulus (E_x^e) is obtained as

$$E_x^e = \frac{(F_1 + F_2 + F_3)}{\Delta_x}. \quad (12)$$

The solutions for the core effective transverse shear moduli (G_{yz}^e and G_{xz}^e) are obtained based on a homogenization method [Xu et al. 2001] and are given as

$$G_{xz}^e = \left(\frac{t_1}{2h} + \frac{bt_2}{2hS} \right) G_{12}^s, \quad G_{yz}^e = \frac{2ht_2}{bS} G_{12}^s, \quad (13)$$

where G_{12}^s is the shear modulus of solid walls (Table 1), and S is the length for the curved segment, $S = \int_A^B ds$ (Figure 5).

Based on the above formulas for both the Young moduli and transverse shear moduli, the equivalent material properties of the sinusoidal core in the longitudinal and transverse directions are provided in Table 3.

1.3. Effective stiffness properties of honeycomb sandwich beams. Next we find the stiffness coefficients of a sandwich panel by modeling the sandwich as a three-layer laminated plate (top and bottom face sheets

E_x^c	E_y^c	G_{xz}^c	G_{yz}^c
0.531 GPa	0.0449 GPa	0.292 GPa	0.119 GPa
7.702×10^4 psi	0.651×10^4 psi	4.235×10^4 psi	1.726×10^4 psi

Table 3. Equivalent material properties of sinusoidal honeycomb core.

and core). Then the constitutive relations for the sandwich deck including the transverse shear deformation are obtained. The in-plane stress-strain relation of a general orthotropic lamina is expressed as

$$\{\sigma\} = [\bar{Q}]\{\varepsilon\}, \quad (14)$$

where, $\{\sigma\} = \{\sigma_x, \sigma_y, \sigma_{xy}\}$, $\{\varepsilon\} = \{\varepsilon_x, \varepsilon_y, \varepsilon_{xy}\}$, and $[\bar{Q}]$ is the matrix of reduced stiffness coefficient \bar{Q}_{ij} . Integration of (14) through the thickness of the beam results in the relation between the resultant forces and moments and the strains and curvatures:

$$\begin{Bmatrix} \{N\} \\ \{M\} \end{Bmatrix} = \begin{bmatrix} [A] & [B] \\ [B] & [D] \end{bmatrix} \begin{Bmatrix} \{\varepsilon\} \\ \{\kappa\} \end{Bmatrix}, \quad (15)$$

where $[A]$ is the 3×3 extensional stiffness sub-matrix, $[B]$ is the 3×3 bending-extension coupling stiffness sub-matrix, $[D]$ is the 3×3 bending stiffness sub-matrix [Jones 1999]. The sandwich beam is symmetric with respect to the middle surface; hence the bending-extension coupling coefficients are zero. The compliance equations are obtained by inverting the matrices in (15):

$$\begin{Bmatrix} \{\varepsilon\} \\ \{\kappa\} \end{Bmatrix} = \begin{bmatrix} [\alpha] & [0] \\ [0] & [\delta] \end{bmatrix} \begin{Bmatrix} \{N\} \\ \{M\} \end{Bmatrix}. \quad (16)$$

To obtain the beam stiffness coefficients from (16), in accordance with Whitney's assumption [1987], only N_x and M_x are retained. Hence, the compliance coefficients for the sandwich beam can be simplified to

$$\begin{Bmatrix} \varepsilon_x^0 \\ \kappa_x \end{Bmatrix} = \begin{bmatrix} \alpha_{11} & 0 \\ 0 & \delta_{11} \end{bmatrix} \begin{Bmatrix} N_x \\ M_x \end{Bmatrix}. \quad (17)$$

Inverting (17) leads to the expression for the force resultant of the sandwich beam as

$$\begin{Bmatrix} N_x \\ M_x \end{Bmatrix} = \begin{bmatrix} \bar{A} & 0 \\ 0 & \bar{D} \end{bmatrix} \begin{Bmatrix} \varepsilon_x^0 \\ \kappa_x \end{Bmatrix}, \quad (18)$$

where \bar{A} and \bar{D} are the extensional and bending stiffnesses of the sandwich beam, and they are defined as $\bar{A} = 1/\alpha_{11} = (A_{11}A_{22} - A_{12}^2)/A_{22}$ and $\bar{D} = 1/\delta_{11} = (D_{11}D_{22} - D_{12}^2)/D_{22}$.

Subsequently, the transverse shear stress resultant is derived by considering the constitutive relations for transverse shear stresses in an orthotropic lamina:

$$\begin{Bmatrix} \sigma_{xz} \\ \sigma_{yz} \end{Bmatrix} = \begin{bmatrix} \bar{Q}_{55} & 0 \\ 0 & \bar{Q}_{44} \end{bmatrix} \begin{Bmatrix} \gamma_{xz} \\ \gamma_{yz} \end{Bmatrix}. \quad (19)$$

Following a similar procedure for the extensional and bending stiffnesses and considering only the resultant component in the x -direction (Q_x) and assuming a constant transverse shear strain through the beam thickness, the constitutive relation for the transverse shear resultant is

$$Q_x = kF\gamma_{xz}, \quad (20)$$

where k is the shear correction factor and F is the transverse shear stiffness.

Thus, from (18) and (20), the constitutive relations of the sandwich beam are expressed as

$$\begin{Bmatrix} N_x \\ M_x \\ Q_x \end{Bmatrix} = \begin{bmatrix} \bar{A} & 0 & 0 \\ 0 & \bar{D} & 0 \\ 0 & 0 & kF \end{bmatrix} \begin{Bmatrix} \varepsilon_x^0 \\ \kappa_x \\ \gamma_{xz} \end{Bmatrix}. \quad (21)$$

In the following, the shear correction factor of a three-layer sandwich beam is derived using the energy equivalence principle. Using two-dimensional equilibrium equations, the shear strain energy is calculated and equated to the shear strain energy obtained from the constitutive relations of (20).

Using the equilibrium equation for the stresses on the xz plane in the absence of body forces and after integrating through the thickness of the section, the shear stress expression becomes

$$\sigma_{xz} = - \int_{-h/2}^z \sigma_{x,x} dz. \quad (22)$$

Substitution of (14) into (22), use of the expression of strains and curvatures in (16), and consideration of the equilibrium equation of a beam (i.e., $N_{x,x} = 0$ and $M_{x,x} = -Q_x$) yields

$$\sigma_{xz} = - \int_{-h/2}^z Q_x z (\bar{Q}_{11} \delta_{11} + \bar{Q}_{12} \delta_{12}) dz. \quad (23)$$

Equation (23) expresses the variation of the transverse shear stress through the thickness of the section. Employing the constitutive relation for the transverse shear given in (19) and assuming σ_{yz} as negligible, the shear strain energy per unit length is obtained as follows:

$$U = \frac{1}{2} \int_{-h/2}^{h/2} \frac{(\sigma_{xz})^2}{\bar{Q}_{55}} dz. \quad (24)$$

Then

$$U = \frac{1}{2} \int_{-h/2}^{h/2} \frac{Q_x^2}{\bar{Q}_{55}} \left(\int_{-h/2}^z z (\bar{Q}_{11} \delta_{11} + \bar{Q}_{12} \delta_{12}) dz \right)^2 dz. \quad (25)$$

Similarly, the constitutive relation of (20), which assumes that the average transverse shear strain is constant through the thickness, results in the shear strain energy per unit length as

$$U = \frac{1}{2} \frac{Q_x^2}{kF}. \quad (26)$$

Equating both strain energies given by (25) and (26), the expression of the effective transverse shear stiffness of the sandwich beams including the shear correction factor is given by

$$kF = (kGA)_{xz} = \left[\int_{-h/2}^{h/2} \frac{1}{\bar{Q}_{55}} \left(\int_{-h/2}^z z (\bar{Q}_{11} \delta_{11} + \bar{Q}_{12} \delta_{12}) dz \right)^2 dz \right]^{-1}. \quad (27)$$

For the sandwich beam application, which consists of three layers (two face sheet layers and one core layer), the effective transverse shear stiffness of the sandwich beam is computed, based on (27), as

$$(kGA)_{xz} = b \left[2 \int_{-h/2}^{-hc/2} \frac{1}{\bar{Q}_{55f}} \left(\int_{-h/2}^z z(\bar{Q}_{11f}\delta_{11} + \bar{Q}_{12f}\delta_{12})dz \right)^2 dz + \int_{-hc/2}^{hc/2} \frac{1}{\bar{Q}_{55c}} \left(\int_{-h/2}^z z(\bar{Q}_{11f}\delta_{11} + \bar{Q}_{12f}\delta_{12})dz + \int_{-h/2}^z z(\bar{Q}_{11c}\delta_{11} + \bar{Q}_{12c}\delta_{12})dz \right)^2 dz \right]^{-1}, \quad (28)$$

and the bending stiffness is computed using (18) as

$$(EI)_x = b\bar{D} = b \frac{(D_{11}D_{22} - D_{12}^2)}{D_{22}}, \quad (29)$$

where h is the thickness of the sandwich; h_c is the thickness of the core; b is the width of the beam; the subscripts f and c stand for the face sheet and the core, respectively; and the other parameters are as explained earlier. Based on (14) and (15) and the equivalent properties of face laminates and cores given in Tables 2 and 3, the beam stiffness properties along the longitudinal and transverse directions are reported in Table 4. These properties, which are shown as plate stiffness in Table 5, are later used for the dynamic response analysis and dynamic impact factor calculations.

Beam	width b	depth d	EI	kGA
Longitudinal	0.334 m	0.105 m	$0.4965 \times 10^6 \text{ N}\cdot\text{m}^2$	$12.323 \times 10^6 \text{ N}$
	13.125 in	4.125 in	$172.883 \times 10^6 \text{ lb}\cdot\text{in}^2$	$2.7706 \times 10^6 \text{ lb}$
Transverse	0.203 m	0.105 m	$0.1900 \times 10^6 \text{ N}\cdot\text{m}^2$	$3.0945 \times 10^6 \text{ N}$
	8.000 in	4.125 in	$66.2012 \times 10^6 \text{ lb}\cdot\text{in}^2$	$0.695 \times 10^6 \text{ lb}$

Table 4. Analytical bending and transverse shear stiffness coefficients of sandwich beams.

A_{11}	A_{12}	A_{22}	A_{66}	D_{11}	D_{12}	D_{22}	D_{66}	A_{44}	A_{55}
in units of 10^9 N/m				in units of 10^6 Nm				in units of 10^6 N/m	
1.62	0.31	1.02	0.0206	1.65	0.31	1.03	0.0508	22.9	55.3

Table 5. Axial, bending and shear stiffnesses of the sandwich panel.

2. Dynamics of sandwich bridge decks

The bridge-vehicle interaction involves dynamics of bridge decks and vehicles. Ignoring the roughness of the deck, the governing equations for sandwich bridge deck dynamics consider the total bending deflection (including shear deformation), w , and the bending slope, ψ_x , ψ_y , and they can be written as follows [Dobyns 1981; Ip and Tse 2001]:

$$\begin{aligned} A_{11} \frac{\partial^2 u_0}{\partial x^2} + A_{66} \frac{\partial^2 u_0}{\partial y^2} + (A_{12} + A_{66}) \frac{\partial^2 v_0}{\partial x \partial y} &= \bar{\rho} \frac{\partial^2 u_0}{\partial t^2}, \\ (A_{12} + A_{66}) \frac{\partial^2 u_0}{\partial x \partial y} + A_{66} \frac{\partial^2 v_0}{\partial x^2} + A_{22} \frac{\partial^2 v_0}{\partial y^2} &= \bar{\rho} \frac{\partial^2 v_0}{\partial t^2}, \end{aligned} \quad (30a)$$

$$D_{11} \frac{\partial^2 \psi_x}{\partial x^2} + D_{66} \frac{\partial^2 \psi_x}{\partial y^2} + (D_{12} + D_{66}) \frac{\partial^2 \psi_y}{\partial x \partial y} - k A_{55} \left(\psi_x + \frac{\partial w}{\partial x} \right) = I \frac{\partial^2 \psi_x}{\partial t^2}, \quad (30b)$$

$$(D_{12} + D_{66}) \frac{\partial^2 \psi_x}{\partial x \partial y} + D_{66} \frac{\partial^2 \psi_y}{\partial x^2} + D_{22} \frac{\partial^2 \psi_y}{\partial y^2} - k A_{44} \left(\psi_y + \frac{\partial w}{\partial y} \right) = I \frac{\partial^2 \psi_y}{\partial t^2},$$

$$k \left[A_{55} \left(\frac{\partial \psi_x}{\partial x} + \frac{\partial^2 w}{\partial x^2} \right) + A_{44} \left(\frac{\partial \psi_y}{\partial y} + \frac{\partial^2 w}{\partial y^2} \right) \right] + q = \bar{\rho} \frac{\partial^2 w}{\partial t^2}, \quad (30c)$$

where A_{ij} ($i, j = 1, 2$, or 6) are the extensional stiffness of the face sheet; A_{44} and A_{55} are the transverse shear stiffnesses of the face sheet, and k is the shear correction factor; D_{ij} ($i, j = 1, 2$, or 6) is the bending stiffness of face sheet; u_0 , v_0 , and w are the mid-surface displacements of the face sheet in the x , y , and z directions, respectively; ψ_x and ψ_y are the rotations of the face sheet; and $\bar{\rho} = \int_{-h_i/2}^{h_i/2} \rho dz$ and $I = \int_{-h_i/2}^{h_i/2} \rho z^2 dz$ (ρ is the individual layer density in the face sheet laminate).

The loading function resulting from a group of moving loads can be written as

$$q = \sum_{l=1}^{N_p} p_l(t) \delta(x - x_l(t)) \delta(y - y_l(t)), \quad (31)$$

where $\{p_l(t), l = 1, 2, \dots, N_p\}$ are the moving loads which are moving as a group at a fixed spacing; $x_l(t)$, $y_l(t)$ is the position of the moving load $p_l(t)$; $\delta(x)$ is the Dirac function.

By modal superposition, the displacement of the orthotropic plate can be written as

$$u_0(x, y, t) = \sum_{m=1}^M \sum_{n=1}^N A_{mn}(t) \cos \frac{m\pi x}{a} \sin \frac{n\pi y}{b},$$

$$v_0(x, y, t) = \sum_{m=1}^M \sum_{n=1}^N B_{mn}(t) \sin \frac{m\pi x}{a} \cos \frac{n\pi y}{b},$$

$$w(x, y, t) = \sum_{m=1}^M \sum_{n=1}^N C_{mn}(t) \sin \frac{m\pi x}{a} \sin \frac{n\pi y}{b}, \quad (32)$$

$$\psi_x(x, y, t) = \sum_{m=1}^M \sum_{n=1}^N D_{mn}(t) \cos \frac{m\pi x}{a} \sin \frac{n\pi y}{b},$$

$$\psi_y(x, y, t) = \sum_{m=1}^M \sum_{n=1}^N E_{mn}(t) \sin \frac{m\pi x}{a} \cos \frac{n\pi y}{b},$$

where $A_{mn}(t)$, $B_{mn}(t)$, $C_{mn}(t)$, $D_{mn}(t)$ and $E_{mn}(t)$ are the time-dependent unknown coefficients to be determined; and M and N are the number of the terms used in the series.

The impact load from the truck can also be represented as

$$q(x, y, t) = \sum_{m=1}^M \sum_{n=1}^N Q_{mn}(t) \sin \left(\frac{m\pi x}{a} \right) \sin \left(\frac{n\pi y}{b} \right). \quad (33)$$

(See Figure 6.)

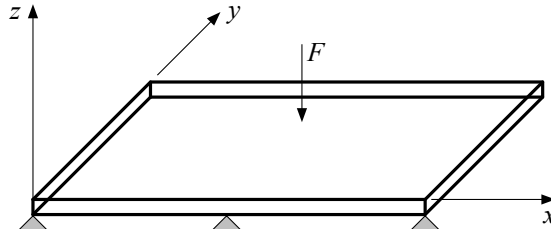


Figure 6. Model of a continuous bridge deck.

In this study, the effects of rotational inertia are neglected ($I = 0$). By considering (30) and (32), an independent set of five equations for each pair (m, n) of Fourier coefficients is obtained,

$$\begin{bmatrix} L_{11} & L_{12} & 0 & 0 & 0 \\ L_{12} & L_{22} & 0 & 0 & 0 \\ 0 & 0 & L_{33} & L_{34} & L_{35} \\ 0 & 0 & L_{34} & L_{44} & L_{45} \\ 0 & 0 & L_{35} & L_{45} & L_{55} \end{bmatrix} \begin{Bmatrix} A_{mn}(t) \\ B_{mn}(t) \\ C_{mn}(t) \\ D_{mn}(t) \\ E_{mn}(t) \end{Bmatrix} = \begin{Bmatrix} 0 \\ 0 \\ Q_{mn}(t) - \rho h \ddot{C}_{mn}(t) \\ 0 \\ 0 \end{Bmatrix}, \quad (34)$$

where the coefficients in the matrix are expressed as

$$\begin{aligned} L_{11} &= A_{11} \left(\frac{m\pi}{a} \right)^2 + A_{66} \left(\frac{n\pi}{b} \right)^2, \\ L_{12} &= (A_{11} + A_{66}) \frac{m\pi}{a} \frac{n\pi}{b}, \\ L_{22} &= A_{22} \left(\frac{n\pi}{b} \right)^2 + A_{66} \left(\frac{m\pi}{a} \right)^2, \\ L_{33} &= k A_{55} \left(\frac{m\pi}{a} \right)^2 + k A_{44} \left(\frac{n\pi}{b} \right)^2, \\ L_{34} &= k A_{55} \frac{m\pi}{a}, \quad L_{35} = k A_{44} \frac{n\pi}{b}, \\ L_{44} &= D_{11} \left(\frac{m\pi}{a} \right)^2 + D_{66} \left(\frac{n\pi}{b} \right)^2 + k A_{55}, \\ L_{45} &= (D_{11} + D_{66}) \frac{m\pi}{a} \frac{n\pi}{b}, \\ L_{55} &= D_{66} \left(\frac{m\pi}{a} \right)^2 + D_{22} \left(\frac{n\pi}{b} \right)^2 + k A_{44}. \end{aligned} \quad (35)$$

Following [Yang and Qiao 2005b], one can reduce (34) to a single differential equation by the transformation

$$A_{mn}(t) = K_{A1} C_{mn}(t), \quad B_{mn}(t) = K_{B1} C_{mn}(t), \quad D_{mn}(t) = K_{A2} C_{mn}(t), \quad E_{mn}(t) = K_{B2} C_{mn}(t), \quad (36)$$

where $K_{A1}, K_{B1}, K_{A2}, K_{B2}$ are the system constants that transform (34) into a single differential equation,

$$\ddot{C}_{mn}(t) + \frac{L_{34}K_{A2} + L_{35}K_{B2} + L_{33}}{\rho h} C_{mn}(t) = \frac{Q_{mn}(t)}{\rho h}. \quad (37)$$

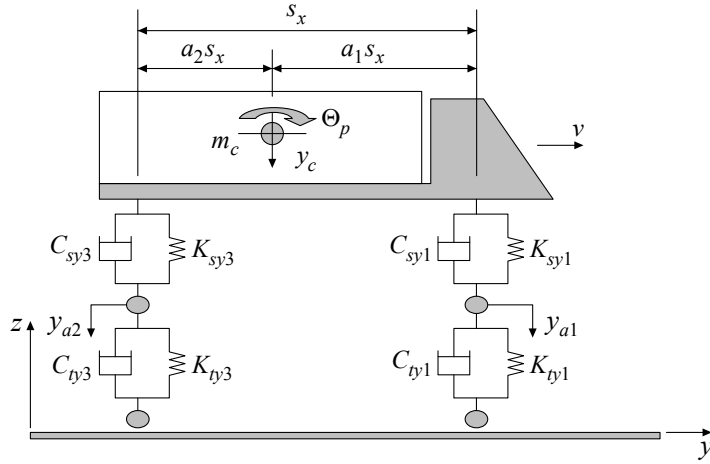


Figure 7. Idealization of two-axle vehicle.

3. Dynamics of vehicles

The mathematical model for the H20-44 truck is shown in [Figure 7](#). The model is similar to that employed in [\[Zhu and Law 2002\]](#).

The vehicle body is assigned three degrees of freedom, corresponding to the vertical displacement (bounce or y), rotation about the transverse axis (pitch or θ_p), and the rotation about the longitudinal axis (roll or θ_r). Each wheel/axle set is described with two additional degrees of freedom in the vertical and roll directions (y_{a1} , y_{a2} , θ_{a1} , θ_{a2}). Therefore, the total number of independent degrees of freedom is seven. The equations of motion of the vehicle are derived using Lagrange's formulation as follows:

$$M_V \ddot{Y} + C_V \dot{Y} + K_V Y = F_V^{\text{int}}, \quad (38)$$

where F_V^{int} is the interaction force vector applied on the vehicle, M_V , C_V and K_V are, respectively, the mass, damping and stiffness matrices of the vehicle system and Y is the vector of the vehicle degrees of freedom.

4. The vehicle-bridge interaction

The vehicle-bridge interaction forces for a single vehicle can be written as

$$\begin{aligned} F_{t1} &= K_{ty1} \left(y_{a1} - \frac{1}{2} S_{d1} \theta_{a1} - w_1 - d_1 \right) + C_{ty1} \left(\dot{y}_{a1} - \frac{1}{2} S_{d1} \dot{\theta}_{a1} - \dot{w}_1 - \dot{d}_1 \right), \\ F_{t2} &= K_{ty2} \left(y_{a1} + \frac{1}{2} S_{d1} \theta_{a1} - w_2 - d_2 \right) + C_{ty2} \left(\dot{y}_{a1} + \frac{1}{2} S_{d1} \dot{\theta}_{a1} - \dot{w}_2 - \dot{d}_2 \right), \\ F_{t3} &= K_{ty3} \left(y_{a2} - \frac{1}{2} S_{d2} \theta_{a2} - w_3 - d_3 \right) + C_{ty3} \left(\dot{y}_{a2} - \frac{1}{2} S_{d2} \dot{\theta}_{a2} - \dot{w}_3 - \dot{d}_3 \right), \\ F_{t4} &= K_{ty4} \left(y_{a2} + \frac{1}{2} S_{d2} \theta_{a2} - w_4 - d_4 \right) + C_{ty4} \left(\dot{y}_{a2} + \frac{1}{2} S_{d2} \dot{\theta}_{a2} - \dot{w}_4 - \dot{d}_4 \right), \end{aligned} \quad (39)$$

where $\{K_{tyi}, i = 1, 2, 3, 4\}$ are the stiffnesses of the tires; $\{C_{tyi}, i = 1, 2, 3, 4\}$ are the friction coefficients of the tires; S_{d1} , S_{d2} are the wheel spacings of the front and rear axles respectively, and

$$w_i = w(x_i(t), y_i(t), t), \tag{40}$$

$$d_i = d(x_i(t), y_i(t), t), \tag{41}$$

where $d(x, y)$ is the surface roughness of the bridge deck (here we assume $d(x, y) = 0$, that is, the surface is smooth), and $(x_i(t), y_i(t))$ is the location of the i -th tire at time t . As the vehicle moves along one lane, we have

$$y_1(t) = y_0 + S_{d1}/2, \quad y_2(t) = y_0 - S_{d1}/2, \quad y_3(t) = y_0 + S_{d2}/2, \quad y_4(t) = y_0 - S_{d2}/2, \tag{42}$$

where y_0 is the transverse coordinate of the centerline of the vehicle.

5. Dynamic responses and dynamic loading factor of different bridge decks

5.1. Vehicle approximated with one degree of freedom. Based on the simply supported boundary conditions we have assumed, the bridge-vehicle interaction model is formulated using (37)–(39) and solved using Newmark- β method [Zhu and Law 2002]. The vehicle body is rigid and subjected to bounce, pitch, and roll motions. The parameters of the vehicle-bridge system for a typical concrete deck are as follows:

l	b	h	E	ν	ρ	m_c	K_{ty}
26.4 m	10.7 m	0.95 m	14.54×10^{10} N/m ²	0.3	2375 kg/m ³	18600 kg	7.85×10^5 N/m

Table 6. Calculation parameters for the concrete deck-vehicle system (where l is the span length, b the bridge width, h the deck thickness, ρ , E and ν the density, Young’s modulus and Poisson’s ratio of the deck material, m_c the mass of the vehicle, and K_{ty} the contact stiffness of tire with the bridge).

The vehicle simulation started from the location of (0, 5.35) and the deflection generated at the center point of the simply supported plate is calculated as shown in Figure 8. The number of Fourier series terms used are 50×50 , which grants its convergence as shown in the sandwich deck case.

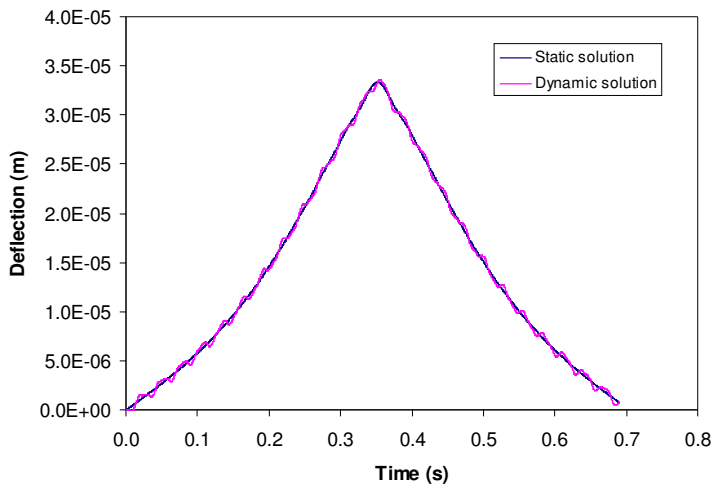


Figure 8. Comparison of the static and dynamic deflection generated by a passing vehicle.

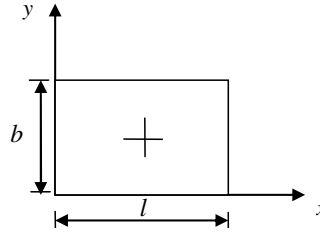


Figure 9. Reference node on the bridge deck.

First the dynamic simulated results are compared with the static results. From [Figure 8](#), we see that the model captures the static and dynamic effect very well. And the peak result is also very close to the numerical result 3.29×10^{-5} m calculated by ABAQUS when the load is applied at the center point.

5.2. Vehicle approximated with seven degrees of freedom. The bridge is still simplified as a simply supported plate. However the vehicle body is approximated as a seven-degree-freedom rigid body and subjected to bounce, pitch and roll motions. The parameters of the vehicle-bridge system are listed in [Tables 7](#) and [8](#).

The dynamic displacement responses of the symbol + on the bridge deck ([Figure 9](#)) under the moving vehicle at speed of 32.5 m/s and 37.5 m/s are shown in [Figure 10](#).

[Figure 10](#) suggests that higher traveling velocities will shorten the time to reach the maximal deflection. Comparing the seven-degree vehicle model with the one-degree vehicle model, it is evident that the seven-degree vehicle model introduces larger vibrations compared to the one-degree model and accurately captures the wheel loads. The wheel loads for $v = 37.5$ m/s are shown in [Figure 11](#). For the given vehicle, the load on the front wheels will be higher, since the gravity center of the vehicle is closer to the front wheels.

l	b	h	E	ν	ρ	S_x	a_1	a_2	S_{d1}	S_{d2}
26.4 m	10.7 m	0.95 m	14.54×10^{10} N/m ²	0.3	2375 kg/m ³	4.73	0.67	0.33	2.05	2.05
m_c	m_{a1}	m_{a2}	I_c	I_t	I_{a1}	I_{a2}	S_{y1}	S_{y2}		
17000 kg	600 kg	1000 kg	9×10^4 kg m ²	1.3×10^4 kg m ²	550 kg m ²	600 kg m ²	1.41 m	1.41 m		

Table 7. Geometric parameters (top row) and mass and inertial parameters (bottom row) for the composite sandwich deck-vehicle system.

K_{sy1}	K_{sy2}	K_{sy3}	K_{sy4}				
1.16×10^5 N/m	1.16×10^5 N/m	3.73×10^5 N/m	3.73×10^5 N/m				
C_{sy1}	C_{sy2}	C_{sy3}	C_{sy4}	C_{ty1}	C_{sy2}	C_{ty3}	C_{ty4}
2.5×10^4	2.5×10^4	3.5×10^4	3.5×10^4	100	100	200	200

Table 8. Spring stiffness in N/m (top row) and damping parameters in Ns/m (bottom row) for the HS20-44 truck.

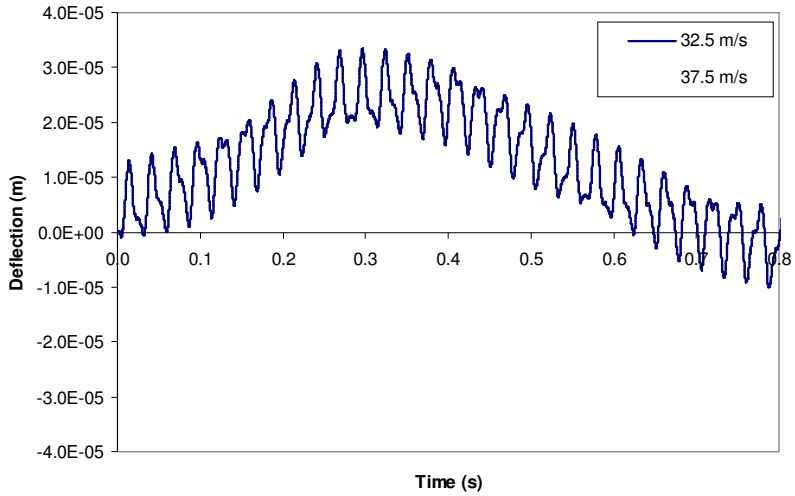


Figure 10. Dynamic displacement time history of the marked position on the composite bridge deck.

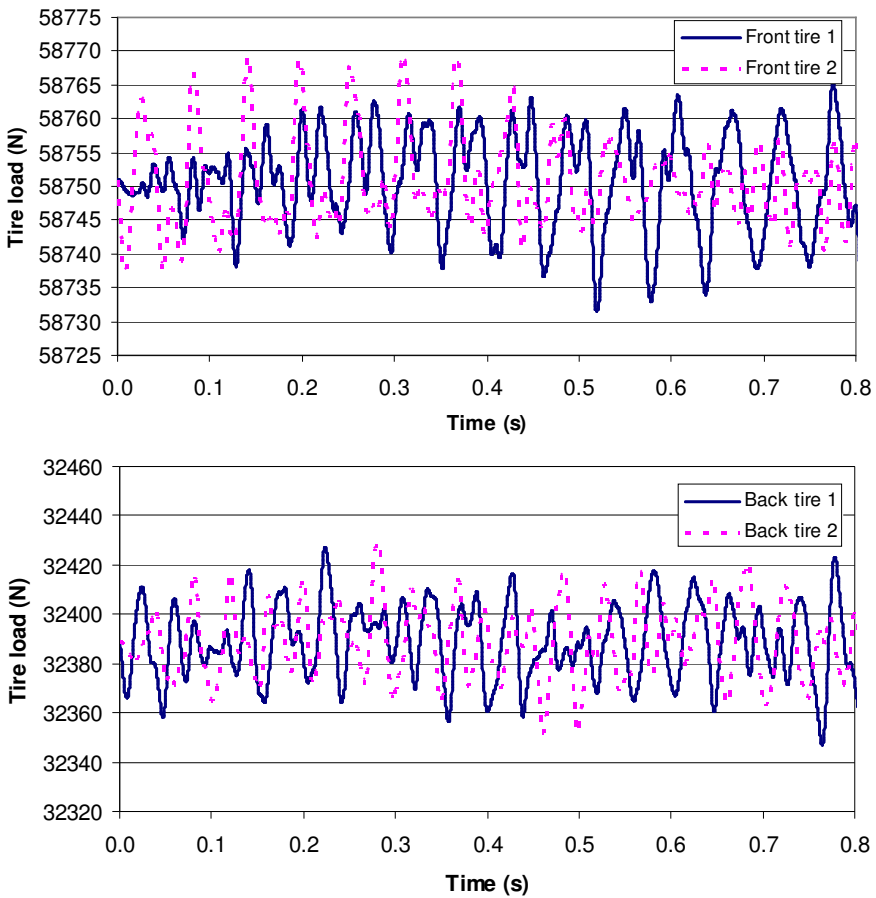


Figure 11. Front wheel (top) and back wheel (bottom) loads of the vehicle.

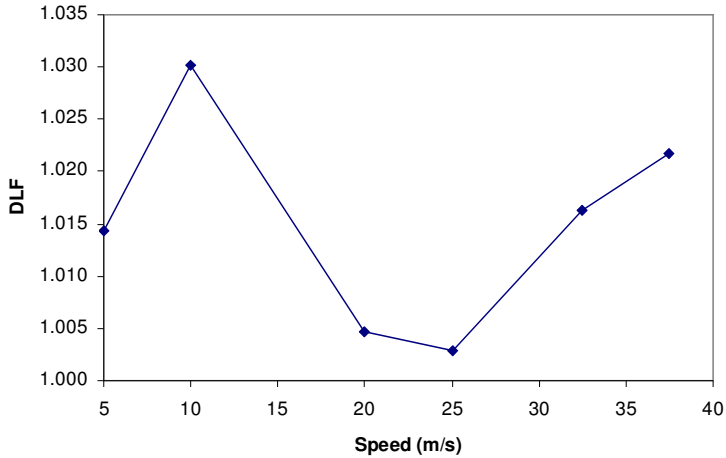


Figure 12. Dynamic load factors of the bridge under given vehicle.

Different dynamic responses will cause different effects on bridge response and need to be considered in design. In order to consider the vehicle-bridge interaction, dynamic loading factor is introduced in many design codes, such as ASSHTO 2002 and ACI 318-05. The dynamic loading factor is defined as the ratio of the maximal dynamic deflection to the maximal static deflection. It is shown in Figure 12 for the center point of the bridge deck considered, taking into account only bridge displacement and ignoring surface roughness.

5.3. Effect of deck stiffness. Using the given sandwich deck as shown in Table 5, the bridge-truck simulation is conducted at a speed $v = 37.5$ m/s. Since the sandwich panel has relatively low stiffness, it is worth verifying the convergence of the solution as a function of the number of terms used. As shown in Figure 13, when the number of terms in each direction reaches 40, the solution converges. Using 50 terms of series in each direction, the center point deflection of the sandwich deck under the given vehicle is shown on Figure 14 with its static maximal deflection as 0.385 m, while the maximal wheel deflection is 0.576 m. From this figure and Figure 15, it is evident that the dynamic load factor (DLF) is 1.50 for the given composite sandwich deck, which is much larger than the design dynamic load factor

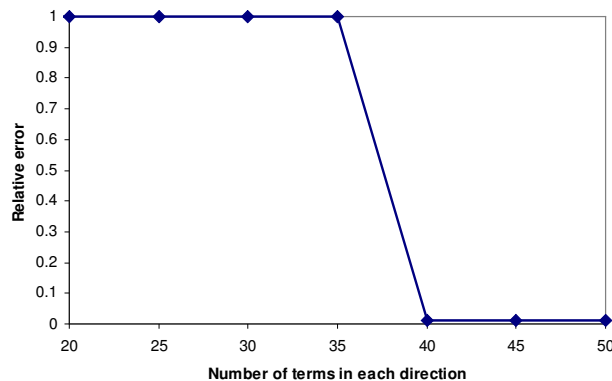


Figure 13. Convergence of the solution.

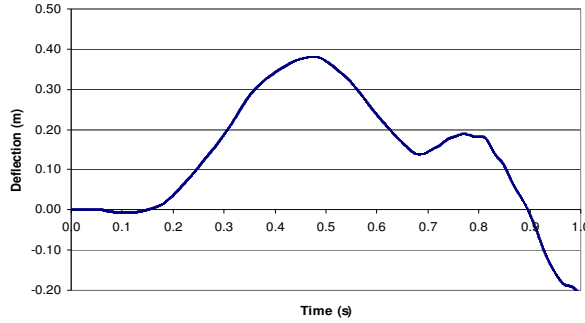


Figure 14. Center deflection history of the sandwich deck panel under the given vehicle.

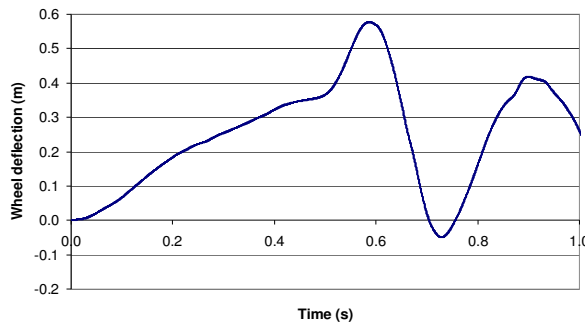


Figure 15. Front wheel deflection of the vehicle considering the sandwich bridge deck and vehicle interaction.

(1.25) for concrete type bridge decks. The reason behind the large deflection and dynamic load factor is that the lower stiffness of the sandwich plays a large role in the bridge-vehicle interaction and needs more attention. Since the maximum dynamic load factor is 1.5, it means that in a linear analysis as used in many codes the maximum stresses in the bridge deck are also 1.5 times those calculated by only considering static loading (neglecting its dynamic effect). Therefore, it is absolutely vital to use dynamic equations when analyzing or designing bridge decks made of composite materials. At the same time, due to large deflections of the composite deck, wheel loads (Figure 16) on the deck are also increased about three times compared to the concrete bridge deck as shown earlier in Figure 11.

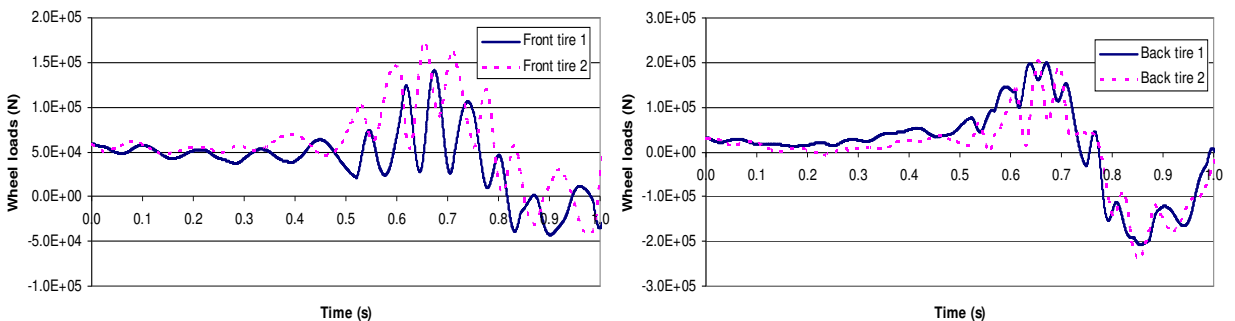


Figure 16. Front wheel (left) and back wheel (right) load of the vehicle.

6. Conclusions

A coupled generalized composite sandwich bridge-vehicle interaction model was introduced capable of capturing the interaction between vehicles and bridge deck systems. The results demonstrate that the proposed dynamic bridge-vehicle interaction procedure using modified Timoshenko plate models can be used to evaluate the dynamic response and the dynamic loading factors of sandwich bridge deck systems. The results suggest that the dynamic load factors vary with traveling speed and increase significantly with decreasing deck stiffness. The proposed model also predicts the increased vibration generated by vehicles. The vehicle simulation model has multi-degrees of freedom and provides estimates of the amplified dynamic loading factor. The procedure described here has potential practical application in the design of sandwich bridge decks.

Acknowledgements

The authors thank Prof. Pizhong Qiao at the Washington State University for his technical support.

References

- [Chamis 1984] C. C. Chamis, “Simplified composites micromechanics equations for strength, fracture toughness, and environmental effects”, technical report TM-83696, NASA, Houston, 1984, available at <http://ntrs.nasa.gov/details.jsp?R=725506>.
- [Davalos et al. 1996] J. F. Davalos, H. A. Salim, P. Z. Qiao, R. Lopez-Anido, and E. J. Barbero, “Analysis and design of pultruded FRP shapes under bending”, *Compos. B Eng. J.* **27**:3–4 (1996), 295–305.
- [Davalos et al. 2001] J. F. Davalos, P. Qiao, X. F. Xu, J. Robinson, and K. E. Barth, “Modeling and characterization of fiber-reinforcement plastic honeycomb sandwich panels for highway bridge applications”, *Compos. Struct.* **52**:3–4 (2001), 441–452.
- [Dobyns 1981] A. L. Dobyns, “Analysis of simply-supported orthotropic plates subject to static and dynamic loads”, *AIAA J.* **19**:5 (1981), 642–650.
- [Frostig 2003] Y. Frostig, “Classical and high-order computational models in the analysis of modern sandwich panels”, *Compos. B Eng. J.* **34**:1 (2003), 83–100.
- [Frostig and Thomsen 2004] Y. Frostig and O. T. Thomsen, “High-order free vibration of sandwich panels with a flexible core”, *Int. J. Solids Struct.* **41**:7 (2004), 1697–1724.
- [Hashin and Rosen 1964] Z. Hashin and B. W. Rosen, “The elastic moduli of fiber-reinforced materials”, *J. Appl. Mech.* **31**:1 (1964), 223–232.
- [Ip and Tse 2001] K. H. Ip and P. C. Tse, “Determination of dynamic flexural and shear moduli of thick composite beam using natural frequencies”, *J. Compos. Mater.* **35**:17 (2001), 1553–1569.
- [Jones 1999] R. M. Jones, *Mechanics of composite materials*, 2nd ed., Taylor & Francis, Philadelphia, 1999.
- [Keller 2001] T. Keller, “Recent all-composite and hybrid fibre-reinforced polymer bridges and building”, *Progress Struct. Eng. Mater.* **3**:2 (2001), 132–140.
- [Librescu and Hause 2000] L. Librescu and T. Hause, “Recent developments in the modeling and behavior of advanced sandwich constructions: a survey”, *Compos. Struct.* **48**:1 (2000), 1–17.
- [Luciano and Barbero 1994] R. Luciano and E. J. Barbero, “Formulas for the stiffness of composites with periodic microstructure”, *Int. J. Solids Struct.* **31**:21 (1994), 2933–2944.
- [Plunkett 1997] J. D. Plunkett, “Fiber-reinforcement polymer honeycomb short span bridge for rapid installation”, IDEA Project Report, NCHRP, Washington, DC, 1997.
- [Qiao and Wang 2005] P. Z. Qiao and J. L. Wang, “On the mechanics of composite sinusoidal honeycomb cores”, *J. Aerospace Eng., ASCE* **18**:1 (2005), 42–50.
- [Whitney 1987] J. M. Whitney, *Structural analysis of laminated anisotropic plates*, Technomic, Lancaster, PA, 1987.

- [Xu et al. 2001] X. F. Xu, P. Qiao, and J. F. Davalos, “Transverse shear stiffness of composite honeycomb core with general configuration”, *J. Eng. Mech.* **127**:11 (2001), 1144–1151.
- [Yang and Qiao 2005a] M. J. Yang and P. Qiao, “Higher-order impact modeling of sandwich beams with flexible core”, *Int. J. Solids Struct.* **42**:20 (2005), 5460–5490.
- [Yang and Qiao 2005b] M. J. Yang and P. Qiao, “Nonlinear impact analysis of fully backed composite sandwich structures”, *Compos. Sci. Technol.* **65**:3–4 (2005), 551–562.
- [Zhu and Law 2002] X. Q. Zhu and S. S. Law, “Dynamic load on continuous multi-lane bridge deck from moving vehicles”, *J. Sound Vib.* **251**:4 (2002), 697–716.

Received 19 Jun 2009. Revised 10 Jan 2010. Accepted 11 Jan 2010.

MIJIA YANG: mijia.yang@utsa.edu

Department of Civil and Environmental Engineering, The University of Texas, San Antonio, TX 78249, United States

A. T. PAPAGIANNAKIS: AT.papagiannakis@utsa.edu

Department of Civil and Environmental Engineering, The University of Texas, San Antonio, TX 78249, United States

JOURNAL OF MECHANICS OF MATERIALS AND STRUCTURES

<http://www.jomms.org>

Founded by Charles R. Steele and Marie-Louise Steele

EDITORS

CHARLES R. STEELE Stanford University, U.S.A.
DAVIDE BIGONI University of Trento, Italy
IWONA JASIUK University of Illinois at Urbana-Champaign, U.S.A.
YASUhide SHINDO Tohoku University, Japan

EDITORIAL BOARD

H. D. BUI École Polytechnique, France
J. P. CARTER University of Sydney, Australia
R. M. CHRISTENSEN Stanford University, U.S.A.
G. M. L. GLADWELL University of Waterloo, Canada
D. H. HODGES Georgia Institute of Technology, U.S.A.
J. HUTCHINSON Harvard University, U.S.A.
C. HWU National Cheng Kung University, R.O. China
B. L. KARIHALOO University of Wales, U.K.
Y. Y. KIM Seoul National University, Republic of Korea
Z. MROZ Academy of Science, Poland
D. PAMPLONA Universidade Católica do Rio de Janeiro, Brazil
M. B. RUBIN Technion, Haifa, Israel
A. N. SHUPIKOV Ukrainian Academy of Sciences, Ukraine
T. TARNAI University Budapest, Hungary
F. Y. M. WAN University of California, Irvine, U.S.A.
P. WRIGGERS Universität Hannover, Germany
W. YANG Tsinghua University, P.R. China
F. ZIEGLER Technische Universität Wien, Austria

PRODUCTION

PAULO NEY DE SOUZA Production Manager
SHEILA NEWBERY Senior Production Editor
SILVIO LEVY Scientific Editor

Cover design: Alex Scorpan


Cover photo: Mando Gomez, www.mandolux.com

See inside back cover or <http://www.jomms.org> for submission guidelines.

JoMMS (ISSN 1559-3959) is published in 10 issues a year. The subscription price for 2010 is US \$500/year for the electronic version, and \$660/year (+\$60 shipping outside the US) for print and electronic. Subscriptions, requests for back issues, and changes of address should be sent to Mathematical Sciences Publishers, Department of Mathematics, University of California, Berkeley, CA 94720-3840.

JoMMS peer-review and production is managed by EditFLOW™ from Mathematical Sciences Publishers.

PUBLISHED BY

 **mathematical sciences publishers**
<http://www.mathscipub.org>

A NON-PROFIT CORPORATION

Typeset in L^AT_EX

©Copyright 2010. Journal of Mechanics of Materials and Structures. All rights reserved.

Mechanical behavior of silica nanoparticle-impregnated kevlar fabrics ZHAOXU DONG, JAMES M. MANIMALA and C. T. SUN	529
A generalized plane strain meshless local Petrov–Galerkin method for the micromechanics of thermomechanical loading of composites ISA AHMADI and MOHAMAD AGHDAM	549
Effective medium theories for wave propagation in two-dimensional random inhomogeneous media JIN-YEON KIM	567
A numerical model for masonry-like structures MAURIZIO ANGELILLO, LUCA CARDAMONE and ANTONIO FORTUNATO	583
A coupled honeycomb composite sandwich bridge-vehicle interaction model MIJIA YANG and A. T. PAPAGIANNAKIS	617
Spectral element approach to wave propagation in uncertain beam structures V. AJITH and S. GOPALAKRISHNAN	637
Energy-minimizing openings around a fixed hole in an elastic plate SHMUEL VIGDERGAUZ	661
Influence of different integral kernels on the solutions of boundary integral equations in plane elasticity Y. Z. CHEN, X. Y. LIN and Z. X. WANG	679